Supporting Information

Elias *et al.* 10.1073/pnas.0811025106

SI Methods

***In Utero* Intraventricular Injection and Electroporation of Plasmid Constructs.** Animals were maintained according to protocols approved by the Institutional Animal Care and Use Committee at the University of California, San Francisco. Intraventricular injections were carried out on E16-timed pregnant Sprague-Dawley rats (41). shRNA oligonucleotides were inserted into pLLox3.7. DNA was prepared in an endotoxin-free manner (Qiagen Endo-free Mega Prep) and mixed with Fast Green dye (Sigma) before surgery. Dams were anesthetized with xylazine/ketamine, and the uterine horns were exposed in a sterile hood environment and hydrated with saline. At a concentration of 1.7 μg/μl, 1 ml of DNA was injected into the left lateral ventricle of all embryos using a bevelled glass micropipet and plunger (Drummond PCR micropipets, 1–10 μl). Immediately after DNA injection, electroporations were performed using an Electro Square Porator ECM830 (BTX Genetronics) (5 pulses, 50 V, 100 ms, 1-s interval). The electroporation tweezertrodes (BTX Genetronics, 7-mm diameter) were orientated such that the positive electrode was adjacent to the right hemisphere and would guide the DNA from the left lateral ventricle into the cortical hem of the developing hippocampus. The uterus was placed back inside the dam, and antibiotic/antimitotic was administered to reduce the chance of infection as well as buprenorphine for pain management. The embryos were allowed to develop up to 17 days after birth. A full video protocol of the *in utero* electroporation process is available; however, the electrodes in the video are oriented to electroporate the cortex and not the medial hem (1).

Live Cell Dye Filling and Confocal Imaging. Neurons were simultaneously filled with dyes for 5–10 min, and slices were immediately fixed with ice-cold 4% paraformaldehyde for 1–3 h, washed two to four times with ice-cold PBS, and imaged. Images were acquired on an Olympus Fluoview 1000 or a Leica TCS SP5 laser-scanning inverted confocal microscope. Images for the quantification of spines in Fig. 3 were collected on the Olympus Fluoview 1000 microscope using the $\times$40 water lens and 0.5-μm z-steps. The 488- and 543-excitation lasers were used to excite Alexa Fluor 488 and Alexa Fluor 568 and were activated sequentially during image collection. Images of electroporated neurons in Fig. S1 were collected on a Leica TCS SP5 microscope using a $\times$10 (numerical aperture = 0.4) air lens or a $\times$63 (numerical aperture = 1.4) oil lens with $\times$1 zoom at the optimum pinhole size and Z-plane interval ($\times$10 lens: 53.04-μm pinhole, 1.315 z-step; $\times$63 lens: 95.49-μm pinhole, 0.118 z-step). The UV and 488-excitation lasers were used to excite DAPI and EGFP, respectively, and were activated sequentially during image collection. The anatomical analysis was carried out in a blind manner. Images were analyzed using Photoshop 7.0. Spine density data are expressed as mean $\pm$ SEM. Statistical significance was determined using two-tail paired *t* tests.

Electrophysiological Recording Conditions.

Dual Whole-Cell Recordings in Acute Slices After Electroporation. Dissection and slicing were carried out in sucrose solution (1–3 °C) consisting of the following (in mM): 87 NaCl, 25 $NaHCO_3$, 75 sucrose, 10 glucose, 2.5 KCl, 1 $NaHPO_4$, 0.5 $CaCl_2$, and 7 $MgCl_2$. Slices were maintained during the day in artificial cerebrospinal fluid (ACSF) between 25 and 28 °C, consisting of the following (in mM): 119 NaCl, 2.5 KCl, 4 $MgSO_4$ (0.1 to measure NMDAR field EPSPs), 1 NaH_2PO_4, 26.2 $NaHCO_3$, 11 glucose, and 4 $CaCl_2$. Sucrose solution and ACSF were saturated with 95% O_2/5% CO_2.

For comparison of AMPAR and NMDAR, EPSC amplitude synaptic responses were recorded simultaneously using the dual whole-cell recording configuration from pairs of adjacent transfected ($EGFP^+$) and untransfected neurons (at most 2 cell bodies apart) following electrical stimulation of a common pathway with a monopolar glass electrode filled with ACSF. The recording glass electrodes (3–5 MΩ) were filled with internal recording solution containing the following (in mM): 125 $CsMeSO_3$, 2.5 CsCl, 7.7 TEA, 5 QX-314, 4 Mg-ATP, 0.3 Na-GTP, 20 Hepes, 8 NaCl, 10 BAPTA, pH 7.2, and 280–290 mOsm.

AMPAR EPSCs were evoked while voltage-clamping cells at $-$70 mV, and the amplitude was determined by measuring the peak of this response. NMDAR EPSCs were evoked while voltage-clamping cells at +40 mV, and NMDAR EPSC amplitudes were determined, depending on the experiments (see text for details), by measuring the amplitude of compound EPSCs 100 ms after the shock artifact or by measuring the peak of the EPSC after blocking the AMPAR component with NBQX. Cell pairs were discarded if either the series or input resistance between cells in a pair differed by more than 20%.

The NMDAR EPSC decay time was determined as a single weighted decay measure calculated from the area under the peak-normalized current for 1.5 s after the peak (7). The percent block by ifenprodil was determined by comparing the NMDAR EPSC peak amplitude 5 min before and 20–25 min after application of ifenprodil. mEPSCs were recorded at $-$70 mV in the presence of 0.5 μM tetrodotoxin, 0.1–0.15 mM picrotoxin, and 50 mM sucrose, and they were analyzed off-line using a threshold of 4 pA. To determine PPR, two EPSCs were evoked with an interpulse interval of 40 ms; PPR was determined as the ratio of the amplitude of the second pulse and the first pulse.

To minimize possible voltage-clamp artifacts that can affect the kinetics of the NMDAR EPSC decay times, the size of the EPSC was typically limited to less than 200 pA.

Pharmacologically isolated NMDAR EPSCs (25 μM NBQX and 0.15 mM picrotoxin) were obtained using somatic whole-cell voltage-clamp recordings from visually identified transfected and untransfected neurons.

Electrophysiological Recordings in Mouse Acute Slices. NMDAR-mediated field EPSP recordings were made in CA1 stratum radiatum following stimulation of Schaffer collaterals with monopolar glass electrodes filled with 1 M NaCl. Field EPSP recordings were done in nominally free magnesium ACSF (0.1 mM $MgSO_4$) supplemented with 25 μM NBQX and 0.1–0.15 mM picrotoxin. Synaptic responses were recorded with glass electrodes (3–5 MΩ) filled with 1 M NaCl using a MultiClamp 700A amplifier (Axon Instruments).

Electrophysiological Recordings in Slice Culture. Five to eight days after preparation, slice cultures were injected near the pyramidal cell layer with Semliki Forest viruses expressing PSD-95-GFP for 18 to 24 h. Recordings were made from pairs of pyramidal neurons using 3–5-MΩ glass electrodes filled with an internal solution containing the following (in mM): 115 $CsMeSO_3$, 20 CsCl, 10 Hepes, 2.5 $MgCl_2$, 4 Mg-ATP, 0.4 Na-GTP, 0.6 EGTA, 5 QX-314, pH 7.2, and 290–300 mOsm. External perfusion medium consisted of the following (in mM): 119 NaCl, 2.5 KCl, 4 $MgSO_4$, 1 NaH_2PO_4, 26.2 $NaHCO_3$, 11 glucose, and 4 $CaCl_2$,

saturated with 95% O_2/5% CO_2 and including 0.1–0.15 picrotoxin and 5–10 μM 2-Chloroadenosine. A cell pair was discarded if either the series or input resistance between cells in the pair differed by more than 20%.

AMPAR EPSCs were evoked while voltage-clamping cells at −70 mV, and the amplitude was determined by measuring the peak of this response. NMDAR EPSCs were obtained while voltage clamping cells at +40 mV, and their amplitudes were determined by measuring the peak of the pharmacologically isolated EPSC (ACSF supplemented with 25 μM NBQX and 0.15 mM picrotoxin). NMDAR EPSC decay times were determined as described previously for acute slices.

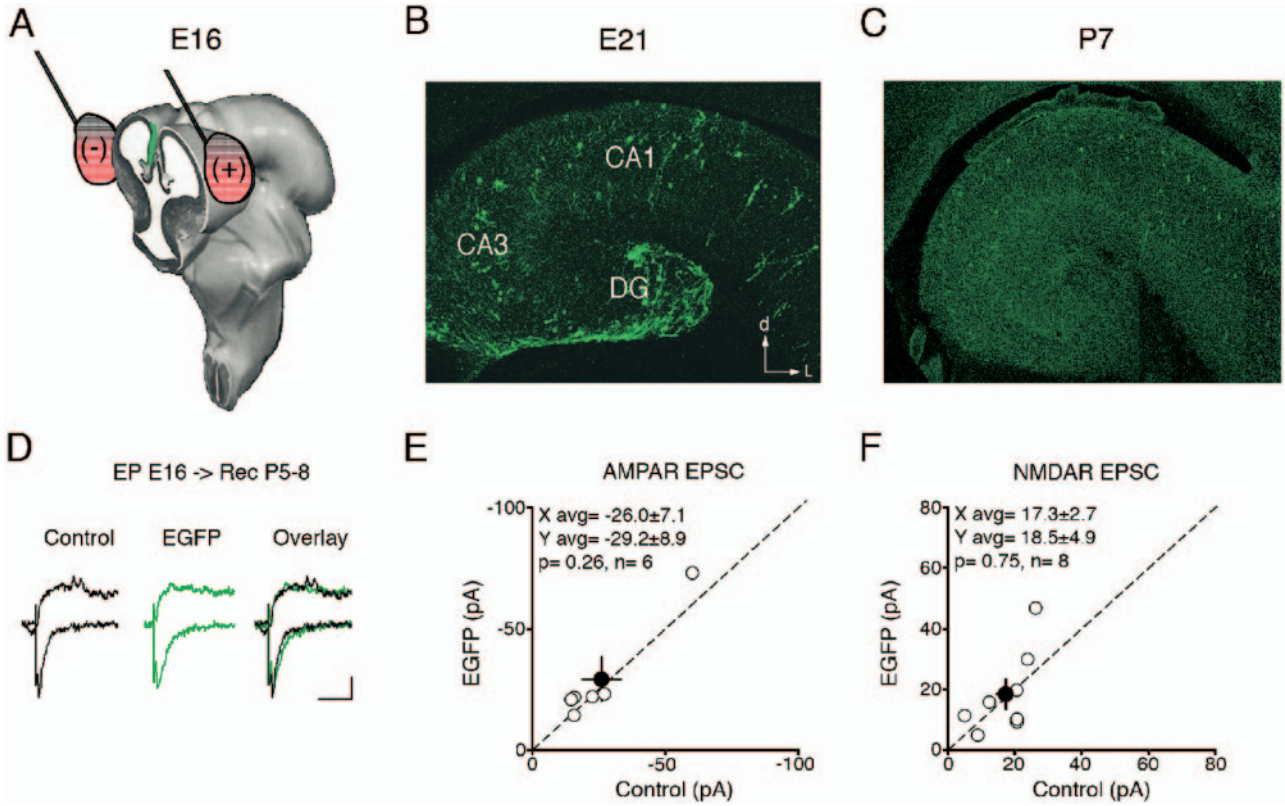

Fig. S1. System to study the molecular mechanisms of synapse development *in vivo*. (*A*) Three-dimensional drawing of a rodent brain at E16 shows the orientation of the (+) and (−) electrode paddles relative to the cortical hem of the developing rat brain. The electroporated region is shown in green. (*B*) Confocal fluorescence image of an E21 hippocampal coronal section from an electroporated brain shows EGFP$^+$ neurons (green) populating the dente gyrus (DG) and CA fields (CA3 and CA1). (*C*) Confocal fluorescence image of an electroporated P7 hippocampus shows a mosaic distribution of EGFP$^+$ neurons throughout the CA fields. (*D*) Electrophysiology traces of evoked EPSCs recorded simultaneously from an untransfected control neuron and an EGFP$^+$ neighbor. (Scale bars: 50 pA, 25 ms.) For scatter plots, open circles represent amplitudes for individual pairs and filled circles represent mean ± SEM. Distributions of AMPAR (*E*) and NMDAR (*F*) EPSC amplitudes.

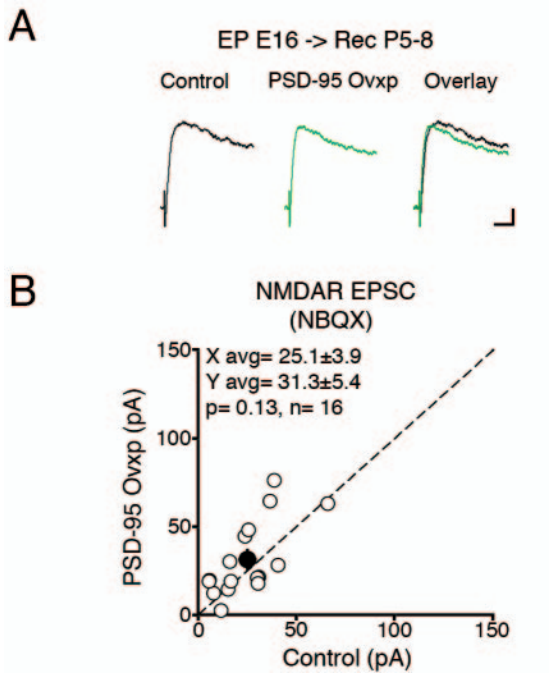

Fig. S2. PSD-95 overexpression during synaptogenesis *in vivo* does not affect the amplitude of pharmacologically isolated NMDAR EPSCs. (*A*) Traces of pharmacologically isolated (25 μM NBQX) NMDAR EPSCs recorded simultaneously from untransfected control and PSD-95 overexpressing neurons. (Scale bars: 10 pA, 25 ms.) (*B*) Distribution of peak NMDAR EPSCs shows no significant difference in amplitude between control and PSD-95 overexpressing neuron pairs.

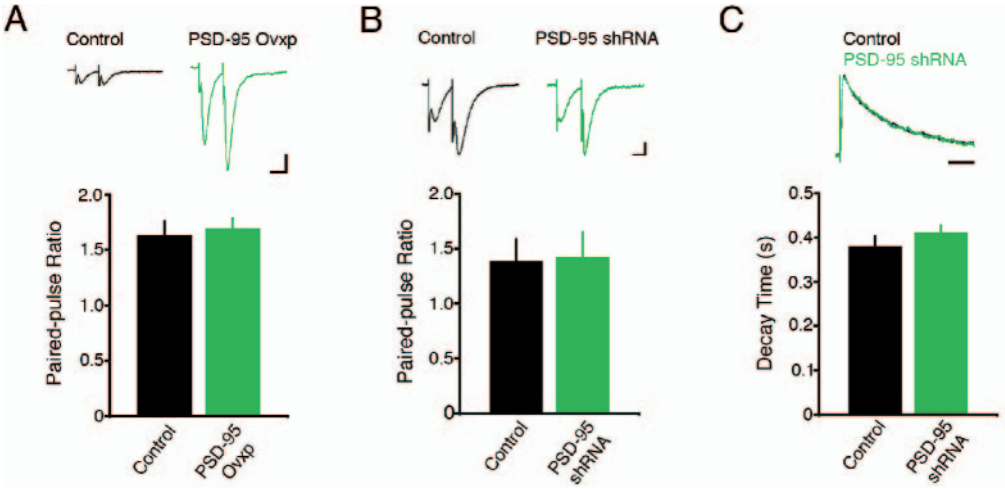

Fig. S3. PSD-95 knockdown during synaptogenesis does not affect synaptic function. Paired-pulse traces (*Top*) and PPR summary bar graph (*Bottom*) show no significant effect of PSD-95 overexpression (*A*: control: 1.63 ± 0.14, $n = 18$; PSD-95 Ovxp: 1.69 ± 0.10, $n = 32$; $P = 0.72$; scale bars: = 50 pA, 25 ms) or knockdown (*B*: control: 1.4 ± 0.29, $n = 7$; PSD-95 shRNA: 1.41 ± 0.24, $n = 7$; $P = 0.93$; scale bars: 25 pA, 20 ms; error bars = SEM). (*C*) (*Top*) Peak-scaled NMDAR EPSCs from a PSD-95 shRNA-expressing neuron and slice-matched untransfected control. (Scale bar: 200 ms.) (*Bottom*) Summary bar graph shows no significant difference in NMDAR EPSC decay time between conditions (control: 0.38 ± 0.02 s, $n = 10$; PSD-95 shRNA: 0.41 ± 0.02 s, $n = 10$; $P = 0.35$).

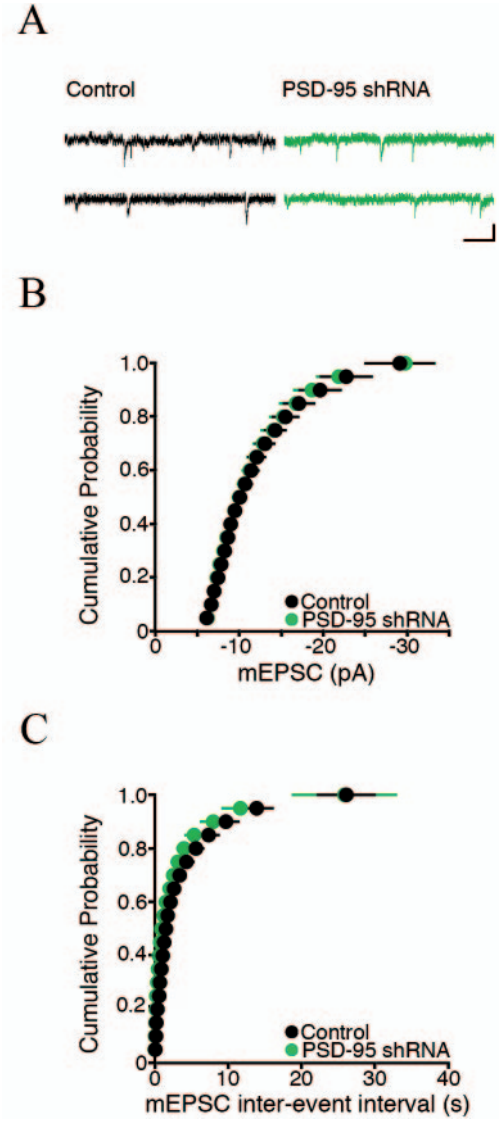

Fig. S4. PSD-95 is not necessary for AMPA receptor synaptic trafficking during synaptogenesis *in vivo*. mEPSC sample traces (*A*: scale bar: 10 pA, 200 ms) and cumulative probability distributions show that shRNA-mediated knockdown of PSD-95 does not affect mEPSC amplitude (*B*: control: $n = 15$; PSD-95 shRNA: $n = 17$; $P = 0.95$) or frequency (*C*: control $n = 15$; PSD-95 shRNA, $n = 17$; $P = 0.2$).

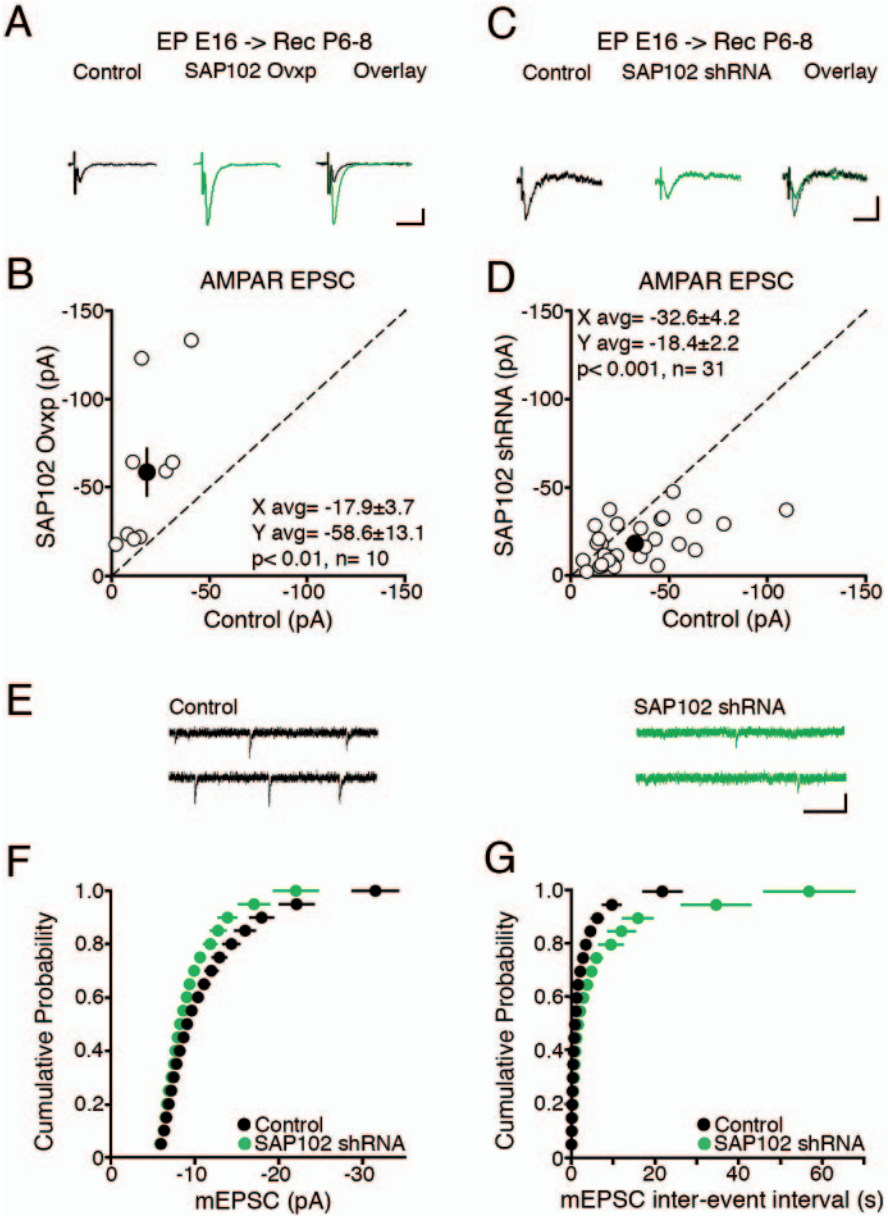

Fig. S5. SAP102 mediates AMPA receptor synaptic trafficking during synaptogenesis *in vivo*. (*A*, *B*) SAP102 overexpression in transfected neurons significantly increases the amplitude of AMPAR EPSCs relative to untransfected control neurons. (*A*) Representative traces of evoked EPSCs in a control untransfected and a neighboring neuron expressing SAP102 shRNA. (Scale bar: 20 pA, 25 ms.) (*C*–*D*) shRNA-mediated knockdown of SAP102 in a transfected neurons significantly reduces the amplitude of AMPAR EPSCs relative to untransfected control neurons. (*E*–*G*) mEPSC sample traces (*E*, scale bar: 10 pA, 200 ms) and cumulative probability distributions show that shRNA-mediated knockdown of SAP102 significantly reduces mEPSC amplitude (*F*: control: $n = 15$; SAP102 shRNA = 11; $P < 0.05$) and frequency (*G*: control: $n = 15$; SAP102 shRNA: $n = 11$; $P < 0.01$). Error bars = SEM.

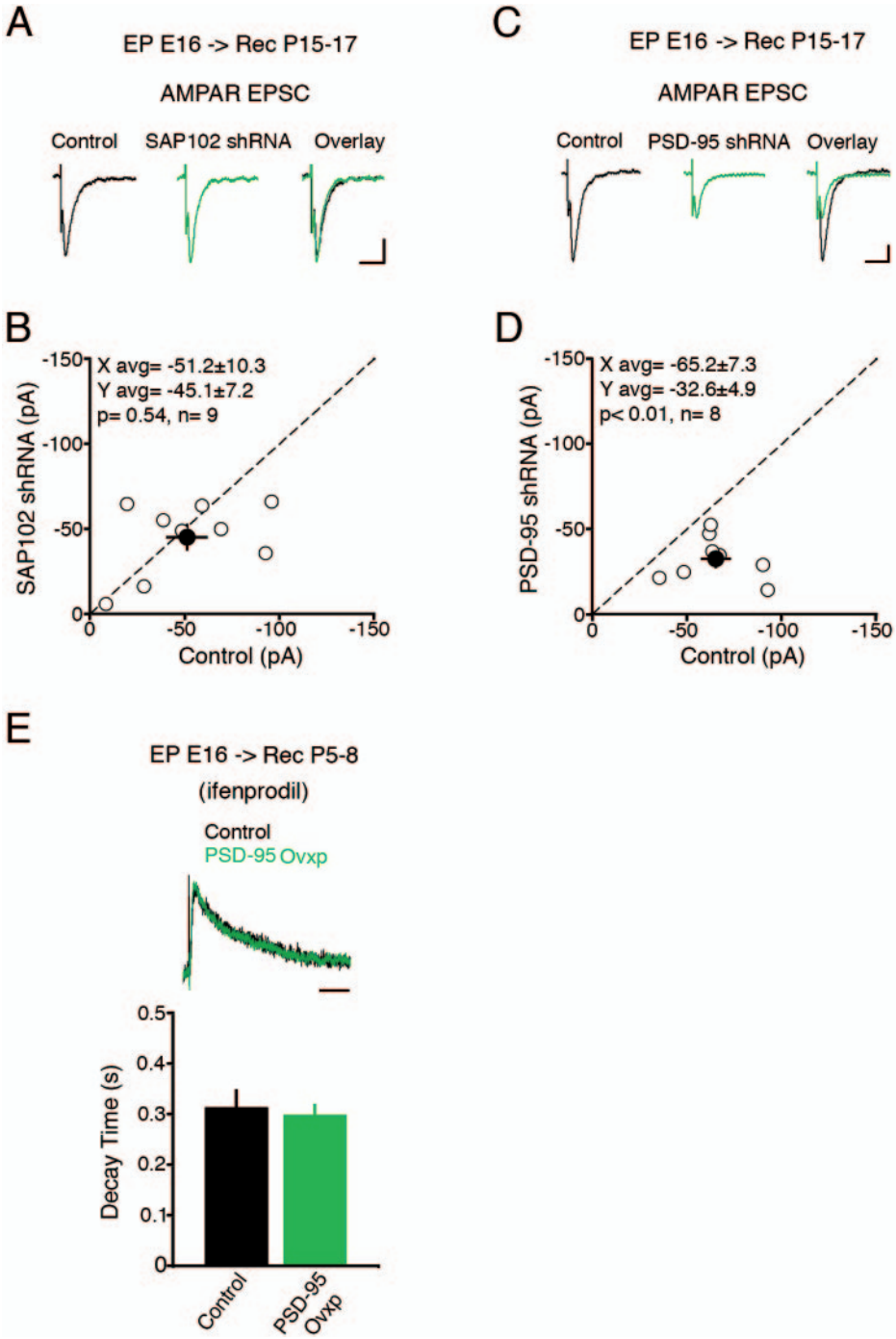

Fig. S6. PSD-95, but not SAP102, is necessary for synaptic maturation of AMPAR-mediated transmission *in vivo*. SAP102 knockdown from E16 to P15–P17 does not impair AMPAR-mediated synaptic transmission. (*A*) Representative traces of evoked AMPAR EPSCs in a control neuron and a neighboring neuron expressing SAP102 shRNA. (*B*) Scatter plot shows no significant difference in the amplitude of AMPAR EPSCs between conditions. (*C*) Representative traces of AMPAR EPSCs recorded simultaneously from untransfected control and PSD-95 shRNA-expressing neurons. (*D*) Scatter plot shows a significant reduction in AMPAR EPSC amplitude in PSD-95 shRNA-expressing neurons relative to adjacent control neurons. (*E*) Sample traces (*Top*) and summary bar graph (*Bottom*) show that the decay time of NMDAR EPSCs recorded in the presence of ifenprodil did not differ in PSD-95 overexpressing neurons (control: 0.31 ± 0.03 s, $n = 8$; PSD-95 Ovxp: 0.29 ± 0.02 s, $n = 12$; $P = 0.69$). (Scale bars: *A* and *C* = 20 pA, 25 ms; *E* = 200 ms.)

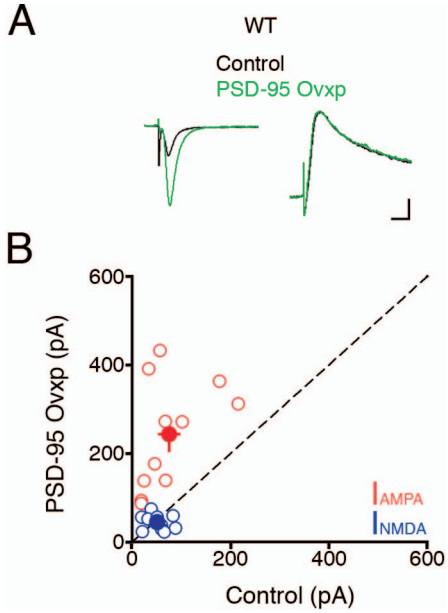

Fig. S7. PSD-95 overexpression enhances AMPAR-mediated synaptic transmission. (*A*) Sample traces of AMPAR EPSCs (*Left*) and NMDAR EPSCs (*Right*) recorded simultaneously from PSD-95 overexpressing (PSD-95 Ovxp) and uninfected control neurons in WT slice cultures. (*B*) Scatter plot (open and filled circles represent amplitudes for single pairs and mean ± SEM, respectively) show that PSD-95 overexpression in WT slice cultures significantly increases AMPAR EPSC (red circles) amplitudes (control: −75.25 ± 19.82 pA; PSD-95 Ovxp: −243.21 ± 37.12 pA; $n = 11$ pairs; $P < 0.001$) without affecting NMDAR EPSC (blue circles) peak amplitudes (control: 50.75 ± 6.95 pA; PSD-95 Ovxp: 44.39 ± 5.13 pA; $n = 11$ pairs; $P = 0.52$). (Scale bars: 50 pA, 25 ms.)